Influence of Tunnel current on DC and Dynamic Properties of Si based Terahertz IMPATT source

Aritra Acharyya [1*], Moumita Mukherjee [2] and J. P. Banerjee [3]
[1, 3] Institute of Radio Physics and Electronics, University of Calcutta, 92, APC Road, Kolkata 700009, India.
[2] Centre of Millimeter wave Semiconductor Devices and Systems, Institute of Radio Physics and Electronics, University of Calcutta, 1, Girish Vidyaratna Lane, Kolkata 700009, India.
[*] E-mail: ari_besu@yahoo.co.in

(Received 06 December 2010; accepted 25 February 2011)

Abstract: The effect of tunneling current on the high frequency properties of double drift (p^+pnn^+) IMPATT devices based on silicon designed to operate at 0.3 THz has been investigated by using a modified double iterative simulation technique. Drift-diffusion model and realistic sharp doping profile of MBE grown junction are used for DC and high frequency analysis of DDR IMPATTs operating in mixed tunneling avalanche transit time (MITATT) mode. The actual rise of junction temperature is estimated through heat flow analysis and considered in the present paper. The DC and high frequency properties of the device in both IMPATT and MITATT modes (with tunneling current) operating in THz regime are studied and compared. The results show that the THz performance of the device as regards power delivery and conversion efficiency deteriorates when tunneling is incorporated in the analysis. This modeling will be helpful to realize Si MITATT source for Terahertz communication systems.

Keywords: Terahertz-source, Silicon, IMPATT and MITATT modes, Tunnel Current.

doi: 10.11906/TST.026-041.2011.03.04

1. Introduction

Terahertz Science and technology is rapidly developing all over the world for its wide-spread application possibilities in both defence and civil sector. Though THz region has several application possibilities, it is not yet been used successfully in all sectors due to lack of suitable THz sources. Most of the available THz sources are complex and bulky. Among two terminal solid-state sources IMPATT diodes have already emerged as high power, high efficiency solid-state sources for mm-wave region [1-3]. Though the conventional IMPATTs are performed successfully, those are limited by power and operating frequency. Recent research is focused on the development of wide-bandgap material (SiC, GaN) based devices for high frequency and high power generation [4-8]. Due to lack of matured fabrication technology SiC and GaN based IMPATTs have not yet been succeeded. From this point of view, the authors have studied the performance of Si IMPATT as possible THz source. Since the bandgap of Si is much less compared to that of SiC or GaN, tunneling may play a role in the THz frequency performance of the devices in MITATT mode. The thinner depletion layer ($W < 0.80\ \mu m$) of mm-wave IMPATT diode and the higher peak electric field ($\xi_m > 6\times10^7\ V/m$) near the junction are the favourable conditions for tunnel generation of electron hole pair (EHP) provided vacant states are available in the conduction band opposite to the filled states of the valance band. Both the carriers generated thorough impact ionization and tunnel generation move in the drift region to produce the necessary transit time delay for IMPATT action. This mode of operation of IMPATT diode is known as mixed tunneling avalanche transit time mode or MITATT mode.

W. T. Read [9] followed by other researchers [10-11] carried out the analysis of IMPATT diode based on the simplifying assumption of equal ionization rates of electrons and holes in the respective semiconductor. Elta and Haddad [12-14] used an effective ionization rate of charge carriers in their analysis by introducing the concept of dead space. Luy *et al* [15] considered a time dependent tunnel current and observed that the DC to RF conversion efficiency of the device decreases due to tunneling induced phase distortion. A generalized method of DC and small-signal analysis based on Gummel-Blue technique [16] was first reported in [17-18], where the authors carried out simulation on the high frequency negative resistivity profiles in the depletion layer of the IMPATT devices. Dash and Pati [19] developed a method of small-signal analysis of Mixed Tunneling and Avalanche Transit Time (MITATT) device on the framework of well-known double iterative field maximum simulation technique first reported by Roy et.al [17-18]. They assumed a junction temperature of 200^0C. Their results show that the influence of tunnel current in MITATT mode causes considerable degradation of the RF performance of the device. In the present paper the authors have adopted a similar approach [19] to carry out the study on terahertz frequency performance of an asymmetrically doped flat-profile Si MITATT device on the framework of Gummel-Blue technique [16].

A detailed numerical simulation of DC and high frequency properties of DDR Si MITATT device designed to operate at 0.3 THz is carried out and the results are presented and compared in this paper. The dependence of tunnel generation rate for electrons on electric field is taken from [20-21]. The tunnel generation rate for holes is calculated from the energy band diagram (Fig. 1) [19]. The present method provides not only the integrated terminal properties of MITATTs such as negative resistance, negative conductance of the device but also the microscopic negative resistance distribution profile in the depletion layer of the device. The effect of tunnel current on RF performance of the device has been determined separately in avalanche and drift zone to identify the region of the depletion layer where the effect is more pronounced.

2. DC and Small-signal Simulation Method

The authors have adopted a double iterative field-maximum method [17-19] to study the MITATT mode operation of the device. MBE growth technique for development of p-n junction in included in the present modeling. At THz region, since the device is operated at a higher bias current density, the junction temperature of the device increases above the room temperature. Thus the authors estimated the rise in junction temperature by considering different layers including the p^+ and n^+ contact metals and adopting one dimensional heat-flow analysis of IMPATT device reported by the authors [22]. It is found that the device junction temperature at 0.3 THz rises to 500 K. Thus the authors have designed the device at 500 K to study the influence of tunnel current in THz IMPATTs. Another consequence of high current operation is that the mobile space charge may degrade the performance seriously [23-24]. The authors have optimized the bias current by several computer runs to minimize the effect of mobile space charge.

One-dimensional model of a reverse biased p^+pnn^+ DDR IMPATT device is shown in Fig. 1. In Fig. 1, x_L/x_R is the position where the electron energy in the valence/conduction band equals the energy corresponding to the bottom/top of the conduction/valance band at the n-side/p-side edge of the depletion layer. W is the total depletion width of the device and x_j is the position of

the *p-n* junction. Poisson's equation including mobile space charge [23-24] in the depletion layer of the diode is,

$$\frac{d\xi}{dx} = \frac{q}{\varepsilon}\left(N_D - N_A + p(x) - n(x)\right) \tag{1}$$

Where, N_D = Ionized donor density, N_A = Ionized acceptor density, so $q.N_{dop} = q.(N_D - N_A)$ = net impurity space charge, $p(x)$ and $n(x)$ are hole and electron densities respectively. ξ_p is the portion of the electric field caused by the space charge of the mobile carriers, thus ξ_p is the total electric field minus the field associated with the impurity space charge [16],

$$\xi_p = \xi - \frac{q}{\varepsilon}\int N_{dop} \quad dx \tag{2}$$

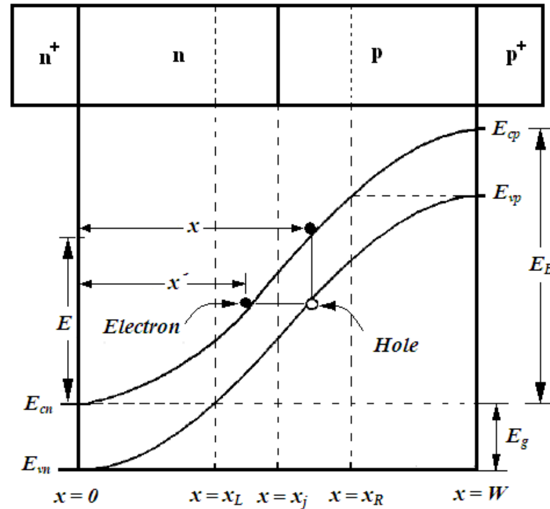

Fig. 1 One-dimensional model of a reverse biased IMPATT Diode [Showing the Tunnelling Positions of Electrons and Holes] [19].

The total current density is the sum of conduction and displacement current densities,

$$J = J_n + J_p + \frac{\partial}{\partial t}(\varepsilon\xi) = q\left(v_p p + v_n n\right) + \frac{\partial}{\partial t}(\varepsilon\xi) \tag{3}$$

Where, $J_p = qv_p p$ = hole current density and $J_n = qv_n n$ = electron current density. Equations (1) and (3) is solved for hole and electron concentrations in terms of the electric field ξ_p and given by [16],

$$p = \frac{J - \left(\frac{\partial}{\partial t} - \varepsilon v_n \frac{\partial}{\partial x}\right)\xi_p}{q\left(v_p + v_n\right)} \tag{4}$$

$$n = \frac{J - \left(\frac{\partial}{\partial t} + \varepsilon v_p \frac{\partial}{\partial x}\right)\xi_p}{q\left(v_p + v_n\right)} \tag{5}$$

Carrier Continuity equations in MITATT mode of operation can be written as,

$$\frac{\partial p}{\partial t} = -\left(\frac{1}{q}\right)\left(\frac{\partial J_p(x)}{\partial x}\right) + G_{Ap}(x) + G_{Tp}(x) + \gamma_p(x) + U_p \tag{6}$$

$$\frac{\partial n}{\partial t} = \left(\frac{1}{q}\right)\left(\frac{\partial J_n(x)}{\partial x}\right) + G_{An}(x) + G_{Tn}(x) + \gamma_n(x) - U_n \tag{7}$$

The avalanche process can be considered as combination of a noiseless generation rate G_A (given by (8)) and a noisy generation rate $\gamma = \gamma_p = \gamma_n$,

$$G_A(x) = G_{An}(x) = G_{Ap}(x) = \alpha_n(x)v_n(x)n(x) + \alpha_p(x)v_p(x)p(x) \tag{8}$$

α_n and α_p are electron and hole ionization rates. v_n and v_p are respective saturated drift velocities. U_n and U_p are the recombination rates of the electrons and holes respectively. Recombination effects are not included in the analysis since the transit time of carriers in the depletion layer of an IMPATT diode is several orders of magnitude shorter than the recombination time. So, the carrier continuity equation in the presence of noise in MITATT mode can be written as,

$$\frac{\partial(p+n)}{\partial t} + \frac{1}{q}\frac{\partial}{\partial x}\left(J_p - J_n\right) = 2\left(G_A(x) + \gamma(x)\right) + G_{Tn}(x) + G_{Tp}(x) \tag{9}$$

In this analysis the tunneling generation rate for electrons [$G_{Tn}(x)$] is obtained from quantum mechanical considerations as reported in [20-21]. Thus,

$$G_{Tn}(x) = a_T \xi^2(x) exp\left(-\frac{b_T}{\xi(x)}\right) \tag{10}$$

Where the coefficients a_T and b_T are,

$$a_T = \frac{q^2}{8\pi^3\hbar^2}\left(\frac{2m^*}{E_g}\right)^{\frac{1}{2}} \tag{11}$$

$$b_T = \frac{1}{2q\hbar}\left(\frac{m^* E_g{}^3}{2}\right)^{\frac{1}{2}} \tag{12}$$

The symbols used in equations (10), (11) and (12) carry their usual significance. The tunneling generation rate for holes can be obtained from Fig. 1. The phenomenon of tunneling is instantaneous and the tunnel generation rate for holes is related with that for electrons i.e. $G_{Tp}(x) = G_{Tn}(x')$. The tunnel generation of an electron at x' is simultaneously associated with the generation of a hole at x, where $(x - x')$ is the spatial separation between the edge of conduction band and valence band at the same energy. If E is the measure of energy from the bottom of the conduction band on the n-side and the vertical difference between x and x' is E_g, x' can be easily obtained from Fig. 1 as [19],

$$x = x'\left(1 - \frac{E_g}{E}\right)^{-\frac{1}{2}} \qquad \text{for } 0 \le x \le x_j \tag{13}$$

$$x = W - \left(W - x'\right)\left(1 + \frac{E_g}{E_B - E}\right)^{-\frac{1}{2}} \qquad \text{for } x_j \le x \le W \tag{14}$$

The hole generation rate due to tunneling is zero in the region defined by $0 \le x \le x_L$ (Fig. 1) as electrons in the valance band have no available states in the conduction band for tunneling. Similarly, non-availability of states in the conduction band for tunneling to take place in the region $x_R \le x \le W$ (Fig. 1) makes no contribution of tunnel generated electrons in this region [19]. The expressions for electron and hole current densities are given by,

$$J_p = qpv_p - qD_p\left(\frac{\partial p}{\partial x}\right) \tag{15}$$

$$J_n = qnv_n + qD_n\left(\frac{\partial n}{\partial x}\right) \tag{16}$$

Where D_n and D_p are the diffusion constants of electrons and holes respectively. In this analysis diffusion current components are neglected for simplicity, as in this case diffusion current components are very much smaller than drift current components. So using the relations $J_n = qnv_n$ and $J_p = qpv_p$ the steady-state carrier continuity equations are written as [Under DC conditions, $\frac{\partial n}{\partial t} = \frac{\partial p}{\partial t} = 0$],

$$\frac{dJ_p(x)}{dx} = \alpha_n(x)J_n(x) + \alpha_p(x)J_p(x) + qG_T(x') + q\gamma(x) \tag{17}$$

$$\frac{dJ_n(x)}{dx} = -\alpha_n(x)J_n(x) - \alpha_p(x)J_p(x) - qG_T(x) - q\gamma(x) \tag{18}$$

The following equations can be formed by using $J = J_n + J_p = Constant$ and $P(x) = [J_p(x) - J_n(x)] / J$ in equations (17) and (18),

$$\frac{\partial P(x)}{\partial x} = \left(\alpha_n + \alpha_p\right) - \left(\alpha_n - \alpha_p\right)P(x) + \frac{q}{2J}\left(G_T(x) + G_T(x')\right) + \frac{2q}{J}\gamma(x) \tag{19}$$

Now $(p - n)$, i.e. the mobile space-charge concentration at any space point can be obtained from (17) and (18) as,

$$q\frac{\partial(p-n)}{\partial x} = J\left(\frac{\alpha_n}{v_n} + \frac{\alpha_p}{v_p}\right) - q\left(\alpha_n - \alpha_p\right)(p - n) + q\left(\frac{G_T(x)}{v_n} + \frac{G_T(x')}{v_p}\right) + q\gamma(x)\left(\frac{1}{v_n} + \frac{1}{v_p}\right) + \frac{\partial \xi}{\partial x}K \tag{20}$$

Where, K is a correction factor whose value depends on the type of the semiconductor base material. In the case on Si, variation of drift velocities for electrons and holes with electric field has form [25],

$$v_{n,p} = v_{sn,sp}\left[1 - exp\left(\frac{-\mu_{n,p}\xi}{v_{sn,sp}}\right)\right] \quad (21)$$

For which the correction factor is given by,

$$K = \frac{J_p\mu_p}{v_p}\left(\frac{1}{v_{sp}} - \frac{1}{v_p}\right) - \frac{J_n\mu_n}{v_n}\left(\frac{1}{v_{sn}} - \frac{1}{v_n}\right) \quad (22)$$

The DC analysis of DDR IMPATT is first carried out by using a double iterative field maximum computer method [17, 19]. In this method the computation starts from the location of field maximum near the metallurgical junction. The spatial distributions of both DC electric field and carrier current densities in the depletion layer are obtained by using the above method, which involves iteration over the magnitude of field maximum (ξ_m) and its location in the depletion layer. A software package has been developed for simultaneous numerical solution of Poisson's equation, combined current continuity equations and the space charge equation subject to appropriate boundary conditions by taking into account the effects of mobile space charge [23-24] and tunneling [19]. Thus the electric field and carrier current density profiles are obtained for DDR device operating in both IMPATT and MITATT modes. The boundary conditions for the electric field at the depletion layer edges are given by (Fig. 2),

$$\xi(0) = 0 \quad and \quad \xi(W) = 0 \quad (23)$$

Where, $x = 0$ and $x = W$ define the p^+ and n^+ edges of the depletion layer. The boundary conditions for normalized current density $P(x) = (J_p - J_n)/J_0$ at the edges are given by,

$$P(0) = \left(\frac{2}{M_p} - 1\right) \quad and \quad P(W) = \left(1 - \frac{2}{M_n}\right) \quad (24)$$

Where, $M_p = J_0 / J_{ps}$ = hole current multiplication factor and $M_n = J_0 / J_{ns}$ = electron current multiplication factor. The necessary device equations are simultaneously solved satisfying the appropriate boundary conditions given in (23) and (24). The field dependence of electron and hole ionization rates (α_n and α_p) and saturated drift velocities of electron (v_{sn}) and holes (v_{sp}) at 500 K are incorporated in the simulation of DC electric field and carrier currents density profiles. The conversion efficiency is calculated from the semi quantitative formula [26],

$$\eta(\%) = \frac{2m}{\pi} \times \frac{V_D}{V_B} \quad (25)$$

Where, V_D = Voltage drop across the drift region, V_B = Breakdown voltage and m is the RF voltage modulation index. Avalanche breakdown takes place when the electric field at the

junction is large enough such that the charge multiplication factors (M_n, M_p) become infinitely large ($\approx 10^6$). The breakdown voltage is obtained by integrating the electric field profile over the total depletion layer width, i.e.,

$$V_B = \int_0^W \xi(x)dx \tag{26}$$

The high-frequency analysis of DDR IMPATT diode is carried out to obtain distribution of negative resistivity in the depletion layer which provides considerable insight into the high frequency performance and the possible measure to improve the same. The range of frequency for which the device exhibits negative conductance is obtained from the admittance plot. The DC parameters are fed as input data for the small signal analysis. The depletion layer edges of the device, are fixed from the DC analysis and taken as the starting and end points for the small signal analysis. Two second order differential equations are framed by resolving the diode impedance $Z(x,\omega)$ into its real part $R(x,\omega)$ and imaginary part $X(x,\omega)$ [18-19] given by,

$$\frac{\partial^2 R}{\partial x^2} + [\alpha_n(x) - \alpha_p(x)]\frac{\partial R}{\partial x} - 2r_n\left(\frac{\omega}{\bar{v}}\right)\frac{\partial X}{\partial x} + \left[\left(\frac{\omega^2}{\bar{v}^2}\right) - H(x) - \frac{qr_p}{\bar{v}\varepsilon}\left(G_T{}'(x) + G_T{}'(x')\right)\right]R - 2\bar{\alpha}\left(\frac{\omega}{\bar{v}}\right)X - 2\left(\frac{\bar{\alpha}}{\bar{v}\varepsilon}\right) = 0 \tag{27}$$

$$\frac{\partial^2 X}{\partial x^2} + [\alpha_n(x) - \alpha_p(x)]\frac{\partial X}{\partial x} - 2r_n\left(\frac{\omega}{\bar{v}}\right)\frac{\partial R}{\partial x} + \left[\left(\frac{\omega^2}{\bar{v}^2}\right) - H(x) - \frac{qr_p}{\bar{v}\varepsilon}\left(G_T{}'(x) + G_T{}'(x')\right)\right]X + 2\bar{\alpha}\left(\frac{\omega}{\bar{v}}\right)R + 2\left(\frac{\omega}{\bar{v}^2\varepsilon}\right) = 0 \tag{28}$$

The boundary conditions for R and X are given by: [n side & p side respectively]

$$\frac{\partial R}{\partial x} + \frac{\omega X}{v_{ns}} = -\left(\frac{1}{v_{ns}\varepsilon}\right) \text{ and } \frac{\partial X}{\partial x} - \frac{\omega R}{v_{ns}} = 0 \qquad \text{at } x = 0 \tag{29}$$

$$\frac{\partial R}{\partial x} - \frac{\omega X}{v_{ps}} = \left(\frac{1}{v_{ps}\varepsilon}\right) \text{ and } \frac{\partial X}{\partial x} + \frac{\omega R}{v_{ps}} = 0 \qquad \text{at } x = W \tag{30}$$

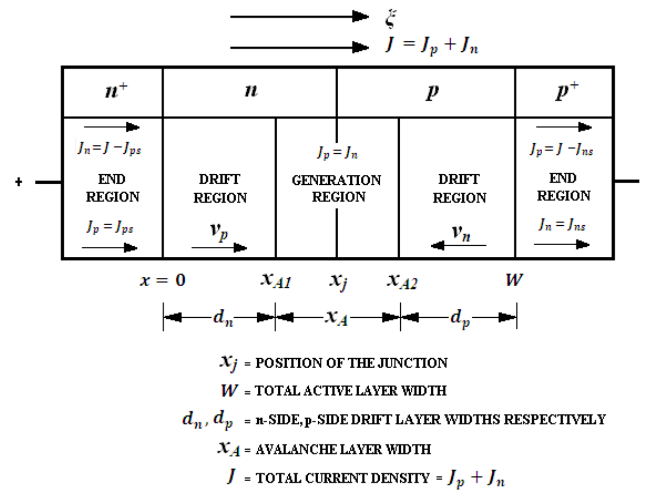

Fig. 2 Different active regions of DDR IMPATT device.

Where, $Z(x,\omega) = R(x,\omega) + i\, X(x,\omega)$. A double-iterative simulation scheme is used to solve those equations (equations (27) & (28)) simultaneously by satisfying the boundary conditions (equations (29) & (30)). The device negative resistance (Z_R) and reactance (Z_x) are computed through the numerical integration of the $R(x)$ and $X(x)$ profiles over the space-charge layer width, W. Thus,

$$Z_R = \int_0^W R dx \quad and \quad Z_X = \int_0^W X dx \tag{31}$$

The negative conductance ($-G$), Susceptance (B) and the quality factor (Q_P) of the device are evaluated by using the following relations:

$$\left| -G(\omega) \right| = \frac{Z_R}{\left(Z_R^{\ 2} + Z_X^{\ 2} \right)} \tag{32}$$

$$\left| B(\omega) \right| = \frac{-Z_X}{\left(Z_R^{\ 2} + Z_X^{\ 2} \right)} \tag{33}$$

$$Q_p = -\left(B / G \right)_{at \quad peak \quad frequency} \tag{34}$$

It may be noted that both $-G$ and B are normalized to the junction area of the diode. At the resonant frequency of oscillation, the maximum RF power output (P_{RF}) from the device is calculated by using the following expression:

$$P_{RF} = \frac{1}{2} . V_{RF}^2 . \left| G_p \right| . A \tag{35}$$

Where, V_{RF} is the amplitude of the RF swing ($V_{RF} = V_B/2$, assuming 50% modulation of the breakdown voltage V_B), G_p is the diode negative conductance at the operating frequency and A is the junction area of the diode.

The present method is free from any simplifying assumptions and it takes into account the MBE grown realistic doping profiles, recently reported values of material parameters of silicon [27] at 500 K and the effect of mobile space charge [23-24].

3. Results and Discussions

A Si DDR IMPATT diode is designed and optimized to operate at 0.3 THz. Simulation studies are carried out for doping and structural parameters listed in Table 1. The method of analysis for MITATT-mode operation presented in the earlier section (Section 2) has been applied to the Si based DDR IMPATT Diode at 0.3 THz. The impact ionization rates and carrier drift velocities of Si are taken from recent reports [25, 27] and are incorporated into the analysis.

DIODE STRUCTURE	**BASE MATERIAL**	***n*-EPITAXIAL LAYER THICKNESS (μm)**	***p*-EPITAXIAL LAYER THICKNESS (μm)**	***n*-EPITAXIAL LAYER DOPING ($\times 10^{23}$ m^{-3})**	***p*-EPITAXIAL LAYER DOPING ($\times 10^{23}$ m^{-3})**	**SUBSTRATE LAYER DOPING ($\times 10^{26}$ m^{-3})**
Flat-DDR	Si	0.1400	0.1100	5.20	6.80	1.0

Table 1 Diode structural and Doping Parameters.

MODE OF OPERATION OF THE DEVICE	**IMPATT MODE**	**MITATT MODE**
BIAS CURRENT DENSITY, J ($\times 10^8$ Amp/m^2)	18.0	18.0
PEAK ELECTRIC FIELD, ξ_m ($\times 10^7$ Volt/m)	8.9500	8.9235
BREAKDOWN VOLTAGE, V_B (Volt)	11.75	11.32
EFFICIENCY, η (%)	6.55	5.89
PEAK OPERATING FREQUENCY, f_p (GHz)	300	480
PEAK CONDUCTANCE, G_P ($\times 10^7$ S/m^2)	-25.1231	-24.1020
PEAK SUSCEPTANCE, B_P ($\times 10^7$ S/m^2)	76.7113	91.6713
QUALITY FACTOR, $Q_P = (-B_P/G_P)$	3.05	3.80
NEGATIVE RESISTANCE, Z_R ($\times 10^{-8}$ Ohm.m^2)	-0.0386	-0.0268
RF OUTPUT POWER DENSITY, P_{RF} ($\times 10^{10}$ Watt/m^2)	0.1385	0.1200

Table 2 Simulated DC and small-signal Parameters.

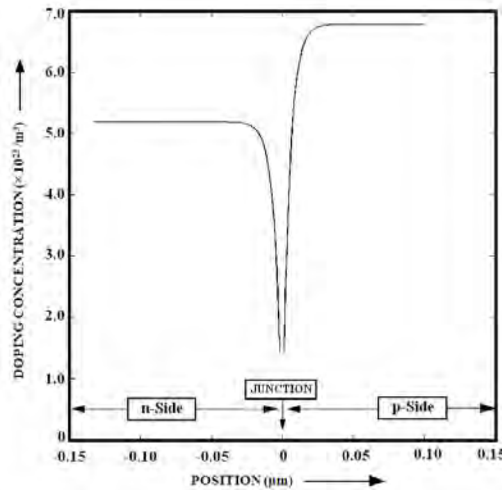

Fig. 3 Doping Profile of the diode.

Doping profile of the designed diode is shown in Fig. 3. Here in our computer program we have incorporated exponential and error-function to get MBE grown realistic doping profile. Electric field and *P(x)*-profiles are given in Fig. 4 and Fig. 5 respectively. Fig. 4 & 5 show that the effect of tunneling current is more prominent near the avalanche region than drift regions; because both electron and hole tunneling generation rate is very high near the junction or high field avalanche region. From the electric field profile it is clear that due to tunneling current electric field at the high field region is lowered. Due to the incorporation of tunneling current efficiency, peak Electric Field and Breakdown voltage of the device decreased, which are easily depicted from Fig. 6.

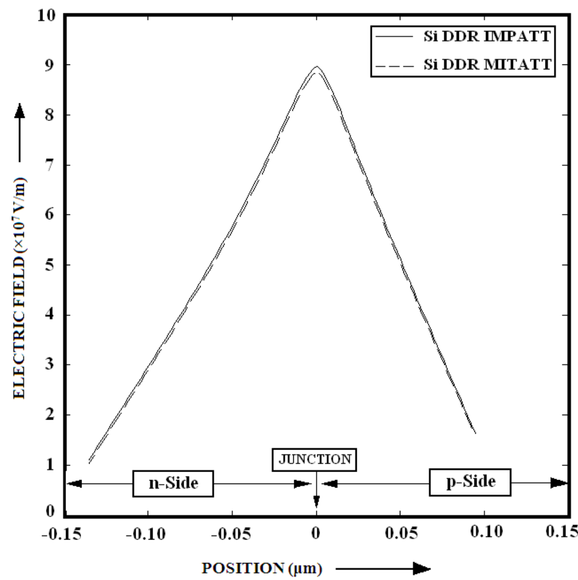

Fig. 4 Electric Field Profiles of the diode in IMPATT and MITATT modes.

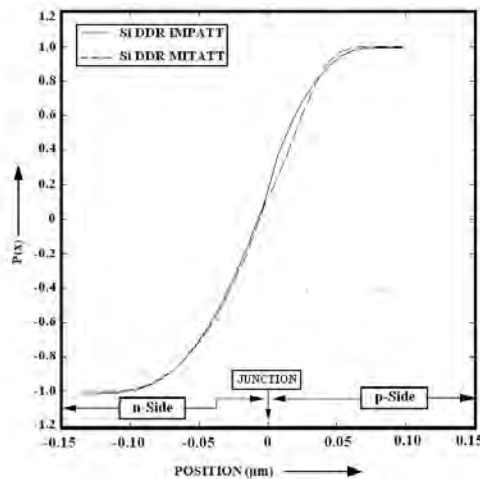

Fig. 5 *P(x)*-Profiles of the diode in IMPATT and MITATT modes.

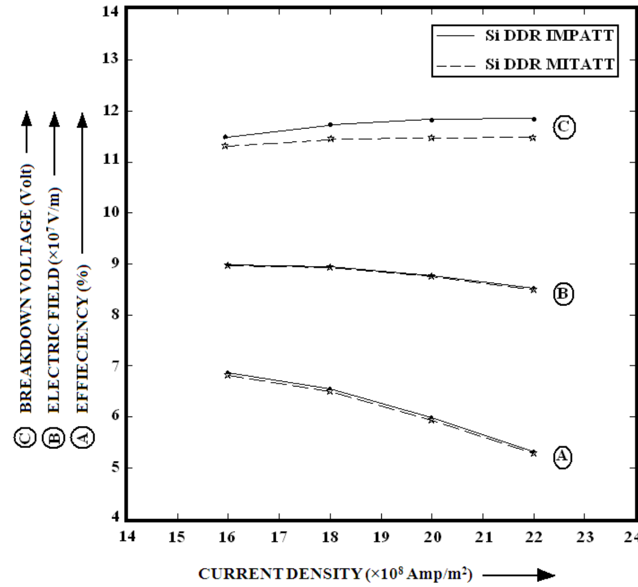

Fig. 6 (A) Efficiency, (B) Peak Electric Field and (C) Breakdown Voltage versus Current Density plots of the diode in IMPATT and MITATT modes.

The admittance characteristics i.e. Conductance-Susceptance Plots of the devices in both IMPATT and MITTAT modes are shown in Fig. 7. It is observed from Fig. 7 that the decrease of the magnitude of negative conductance is 4.06% in Si DDR. The optimum frequency of the device found to be shifted from 0.3 THz (IMPATT mode) to 0.48 THz. Q-factor of the device is an indicator of the growth rate and stability of oscillation. Lower Q-factor close to unity leads to better RF performance of the device. Table 2 shows that the Q-factor of the device degrades in MITATT mode.

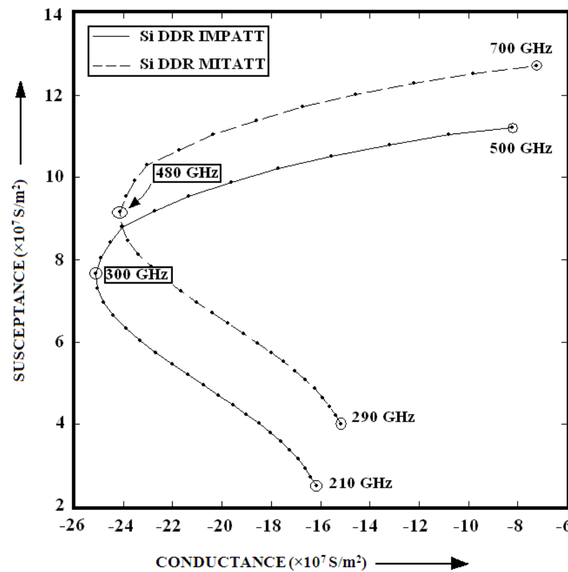

Fig. 7 Small-Signal Conductance versus Susceptance plots of the diode in IMPATT and MITATT modes.

The negative resistivity profile of the DDR device in both IMPATT and MITATT modes are shown in Fig. 8, which exhibit two peaks in the two drift regions separated by a minimum near the junction. The magnitude of negative resistivity peak of the device is higher in n-side than p-side for Si DDR. Ratio of the negative resistivity peaks on n-side and p-side is indirectly connected to the ratio of electron to hole ionization rates of respective materials [28]. It is well known that in Si, α_n is greater than α_p, That is why the magnitude of negative resistivity peak is found to be higher in n-side of the device compared to p-side of it. It is interesting to observe that the magnitude of negative resistance falls appreciably due to the effect of tunneling.

It may further be noted that the decrease in the magnitude of the negative resistance peak due to tunneling is more appreciable on p-side of the device than on the n-side. This can be understood by considering that the tunnel generation rate due to electrons at any point x depends on the electric field at the same point x while tunnel generation rate due to holes at x depends on the electric field at some other point x', given in equations (13) & (14). Thus the tunneling generation rate of electrons attains its peak value close to the junction while that of holes attains the peak value slightly away from the junction on the p-side [Fig. 11] due to the effect of tunneling. The effective tunneling generation rate defined as, $q(G_T(x)+G_T(x'))$ is found to be predominant on p-side of the avalanche zone [19].

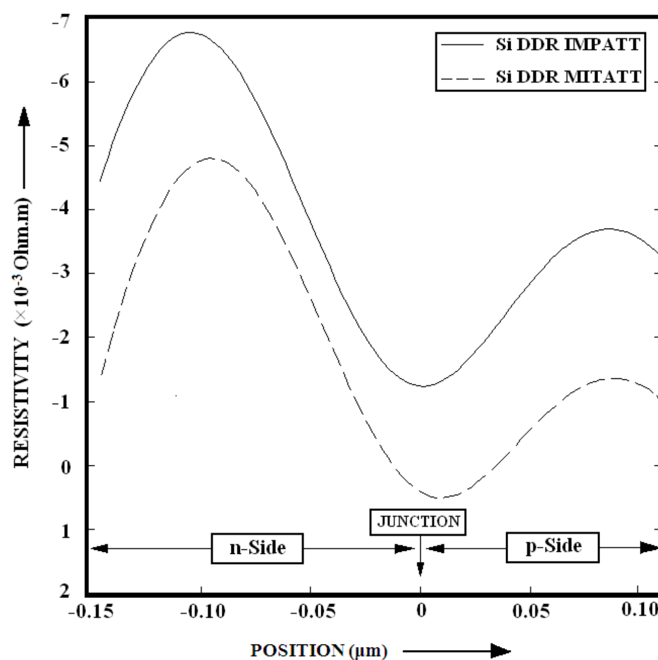

Fig. 8 Negative Resistivity profiles of the diode in IMPATT and MITATT modes.

Fig. 9 shows that the tunneling generation rate increases sharply with electric field in the device under consideration. Fig. 10 shows the spatial variation of both avalanche generation rate and tunneling generation rate in the depletion layer of the device. These generation rates exhibit peaks near the junction plane followed by sharp falls on either side of the junction. In this case, it is clear that the tunneling generation is dominant over avalanche generation (Fig. 10). Since tunneling generation is a strong increasing function of electric field (Fig. 9) that is why for high

frequency operation where electric field near the junction is very high ($\xi \approx 9\times10^{7}$ V/m) tunneling phenomena dominates over the avalanche phenomena. Values of effective mass m^{*} and band gap energy E_g used are respectively $0.137m_0$ and $1.12eV$ for Si [19, 27]. Where the rest mass of the electron, $m_0 = 9.11\times10^{-31}$ Kg.

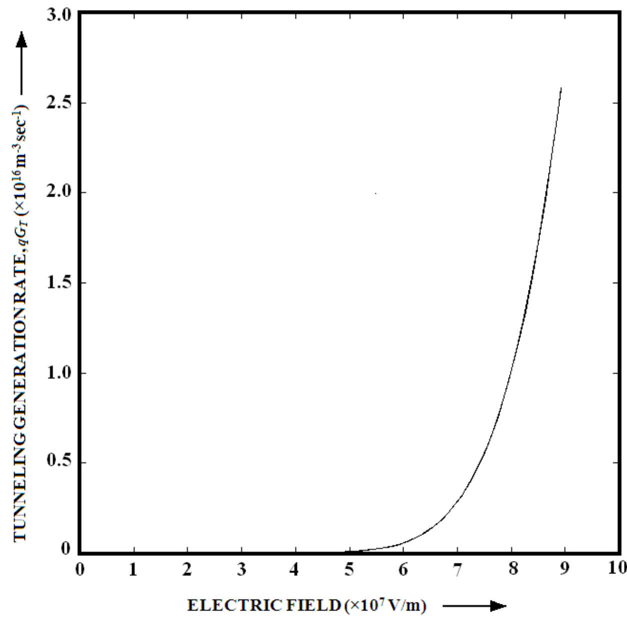

Fig. 9 Tunneling Generation Rate (qG_T) versus Electric Field.

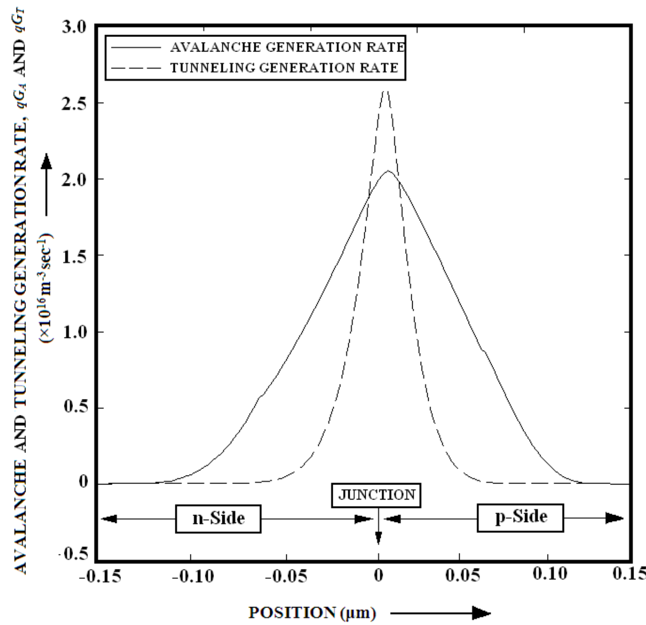

Fig. 10 Spatial variation of Avalanche and Tunnelling Generation Rates [qG_A and qG_T] in the active layers of the diode.

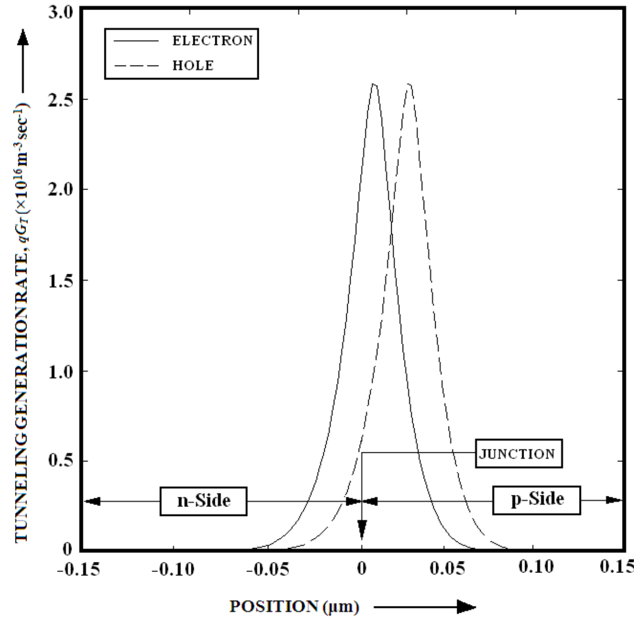

Fig. 11 Spatial variation of Tunnelling Generation Rates of electrons and holes [qG_{Tn} and qG_{Tp}] in the active layers of the diode.

It can be observed from Table 2 that the RF power output of the device decreases in MITATT mode as compared to IMPATT mode. Maximum power output can be obtained from an IMPATT device when the phase difference between total current and AC voltage is 180°. In IMPATT mode of operation, total current gets 180° phase difference with RF voltage due to both avalanche build-up and transit time of charge carriers, while in MITATT mode tunnel current develops the phase delay with RF voltage due to only the transit time. This fact causes phase distortion between the total current and AC voltage leading to lower RF power output of the device.

4. Conclusions

The present study on Si DDR IMPATT predicts the suitability of Si IMPATT as THz source. Results show that the tunnel current degrades the device performance as regards DC to RF conversion efficiency, RF power output etc due to tunneling induced phase distortion. Further the design data, presented in this paper, will be helpful to realize Si based IMPATT oscillators for Terahertz communication.

References

[1] T. A. Midford and R. L. Bernick, “Millimeter Wave CW IMPATT diodes and Oscillators”, *IEEE Trans. Microwave Theory Tech.*, vol. 27, pp. 483-492, (1979).

[2] Y. Chang, J. M. Hellum, J. A. Paul and K. P. Weller, "Millimeter-Wave IMPATT Sources for Communication Applications", *IEEE MTT-S International Microwave Symposium Digest*, pp. 216-219, (1977).

[3] W. W. Gray, L. Kikushima, N. P. Morentc and R. J. Wagner, "Applying IMPATT Power Sources to Modern Microwave Systems". *IEEE Journal of Solid-State Circuits*, vol. 4, pp. 409-413, (1969).

[4] M. Mukherjee, S. Banerjee and J. P. Banerjee, "Dynamic Characteristics of III-V and IV-IV Semiconductor Based Transit Time Devices in the Terahertz Regime: A Comparative Analysis", *Terahertz Science and Technology*, vol. 3, pp 97-109, (2010).

[5] M. Mukherjee, J. P. Banerjee, "DDR Pulsed IMPATT Sources at MM-Wave Window Frequency: High-Power Operation Mode", *International Journal of Advanced Science and Technology*, vol. 19, pp 1-11, (2010).

[6] S. Banerjee, M. Mukherjee and J. P. Banerjee, "Bias current optimization of Wurtzite-GaN DDR IMPATT diode for high power operation at THz frequencies", *International Journal of Advanced Science and Technology*, vol. 16, pp 11-20, (2010).

[7] M. Mukherjee, S. K. Roy, "Wide band gap III-V Nitride based avalanche transit time diode in Terahertz regime: Studies on the effect of punch-through on high frequency characteristics and parasitic series resistance of the devices", *Current Applied Physics*, vol. 10, pp 646-651, (2009).

[8] M. Mukherjee, N. Mazumder, "Modeling of high power 0.3 THz IMPATT oscillator based on 3C-SiC and growth of 3CSiC on Si <100> substrate for possible IMPATT fabrication", *ICMMT*, (2008).

[9] W. T. Read, "A proposed high-frequency negative-resistance diode", *Bell Syst. Tech. J.*, vol. 37, pp. 401-466, (1958).

[10] S. P. Kwok and G. I. Haddad, 'Effect of tunneling on an Impatt oscillator', *J. Appl. Phys.*, 43, 3824-3830, (1972).

[11] M. Chive, E. Constant, M. Lefebvre and J. Pribetich, "Effect of tunneling on high efficiency IMPATT avalanche diode", *Proc. IEEE (Lett.)*, vol. 63, pp. 824-826, (1975).

[12] M. E. Elta and G. I. Haddad, "Mixed tunneling and avalanche mechanism in p-n junctions and their effects on microwave transit time devices", *IEEE Trans. Electron Devices*, vol. 25, pp. 694-702, (1978).

[13] M. E. Elta and G. I. Haddad, "High-frequency limitations of IMPATT, MITATT, and TUNNETT mode devices", *IEEE Trans. Microwave Theory Tech.*, vol. 27, pp. 442-449, (1979).

[14] M. E. Elta and G. I. Haddad, "Large-signal performance of microwave transit-time devices in mixed tunneling and avalanche breakdown", *IEEE Trans. Electron Devices*, vol. 26, 941-948, (1979).

[15] J. F. Luy and R. Kuehnf, "Tunneling assisted Impatt operation", *IEEE Trans. Electron Devices*, vol. 36, pp. 589-595, (1989).

[16] H. K. Gummel and J. L. Blue, "A small-signal theory of avalanche noise in IMPATT diodes", *IEEE Trans. on Electron Devices*, vol. 14, no. 9, pp. 569-580, (1967).

[17] S. K. Roy, M. Sridharan, R. Ghosh, and B. B. Pal, "Computer methods for the dc field and carrier current profiles in impatt devices starting from the field extremum in the depletion layer", *Proc. of NASECODE-I Conf. on Numerical Analysis of Semiconductor Devices (Dublin: Boole Press)*, pp. 266, (1979).

[18] S. K. Roy, J. P. Banerjee and S. P. Pati, "A computer analysis of the distribution of high frequency negative resistance in the depletion layers of impatt diodes", *Proc. of NASECODE-IV Conf. on Numerical Analysis of Semiconductor Devices (Dublin: Boole Press)*, pp. 494, (1985).

[19] G. N. Dash and S. P. Pati, "A generalized simulation method for MITATT-mode operation and studies on the influence of tunnel current on IMPATT properties", *Semicond. Sci. Technology*, vol. 7, pp. 222-230, (1992).

[20] M. E. Elta, "The effect of mixed tunneling and avalanche breakdown on microwave transit-time diodes", Ph.D. dissertation, Electron Physics Lab., Univ. of Mich., Ann Arbor, MI, Tech. Rep, (1978).

[21] E. O. Kane, "Theory of tunneling", *J. Appl. Phys.*, vol. 32, pp. 83-91, (1961).

[22] M. Mukherjee and J. P. Banerjee, "DDR Pulsed IMPATT Sources at MM-Wave Window Frequency: High-Power Operation Mode", *International Journal of Advanced Science and Technology*, vol. 19, pp. 1-11, (2010).

[23] M. Sridharan, and S. K. Roy, "Computer studies on the widening of the avalanche zone and decrease on efficiency in silicon X-band sym. DDR", *Electron Lett.*, vol. 14, pp. 635-637, (1978).

[24] M. Sridharan, and S. K. Roy, "Effect of mobile space charge on the small signal admittance of silicon DDR", *Solid State Electron*, vol. 23, pp. 1001-1003, (1980).

[25] C. Canali, G. Ottaviani and A. A. Quaranta, "Drift velocity of electrons and holes and associated anisotropic effects in silicon", *J. Phys. Chem. Solids*, vol. 32, pp. 1707-1720, (1971).

[26] D. L. Scharfetter and H. K. Gummel, "Large-Signal Analysis of a Silicon Read Diode Oscillator", *IEEE Trans. on Electron Devices*, vol. 16, pp. 64-77, (1969).

[27] 'Electronic Archive: New Semiconductor Materials, Characteristics and Properties', http://www.ioffe.ru/SVA/NSM/Semicond/Si/index.html.

[28] J. P. Banerjee, S. P. Pati and S. K. Roy, "High frequency characterization of double drift region InP and GaAs diodes", *Appl. Phys. A*, vol. 48, no. 5, pp. 437-443, (1989).